Eur. Phys. J. D **39**, 75–85 (2006)
DOI: 10.1140/epjd/e2006-00077-3

THE EUROPEAN PHYSICAL JOURNAL D

Suppression of limit cycles in a free electron laser

C. Bruni[1,a], S. Bielawski[2], G.L. Orlandi[1], D. Garzella[1], and M.E. Couprie[1]

[1] CEA/DSM/DRECAM/SPAM, bâtiment 522, 91191 Gif-sur-Yvette, France
and
LURE, bâtiment 209D, Université Paris-Sud, B.P. 34, 91898 Orsay Cedex, France
[2] PhLAM-CERLA, Université des Sciences et Technologies de Lille, 59655 Villeneuve d'Ascq Cedex, France

Received 23 May 2005
Published online 11 April 2006 –

Abstract. To take complete benefit of the Free Electron Laser (FEL) features, we have developed a feedback control scheme designed to suppress the dynamical instabilities affecting the FEL output intensity. The principle is to stabilize an unstable stationary state that coexists with the unwanted limit cycle. This paper gives a theoretical and experimental description of the stabilized stationary regime of a storage ring FEL in presence of the feedback control. We present a numerical model of the FEL with control, that describes the longitudinal dynamics of the laser pulse in condition of detuning between the FEL and the electron beam. These theoretical results are compared with experiments performed on the Super-ACO FEL. The established feedback control provides stable operation of the FEL.

PACS. 41.60.Cr Free-electron lasers – 42.65.Sf Dynamics of nonlinear optical systems; optical instabilities, optical chaos and complexity, and optical spatio-temporal dynamics

1 Introduction

In order to convert chaotic behavior into periodic motion, Ott, Grebogi and Yorke [1] proposed to use a particular type of feedback control. The core idea is to take advantage of the preexistence of unstable periodic orbits in any chaotic attractor, together with the fact that it is possible to stabilize one of these orbits using conventional feedback control.

Since the first experimental demonstration on a magnetoelastic ribbon by Ditto et al. [2], chaos control has been implemented with success on many systems, in particular in electronics [3,4], lasers [5–8], chemistry [9], hydrodynamics [10], and for controlling cardiac tissues [11] (see Ref. [12] for a review).

The work of Ott, Grebogi and Yorke not only led to an extensive activity on chaos control. It also implicitly emphasized the fact that unstable states (periodic or not, embedded or not in a chaotic attractor, or in the absence of chaos) are potentially useful in general because they can be typically stabilized by a feedback loop involving only small perturbations on a control parameter. Thus there has been an increase of interest for the stabilization of steady states in various situations [13–17].

In this paper we consider the stabilization of Storage Ring Free Electron Lasers [18,19] (SRFEL), that are known to present dynamical regimes leading to a pulsed behavior [20], nefast for FEL use. First experimental control of the limit cycles has been done on the Super-ACO SRFEL [18], on the ELETTRA SRFEL [21] and recently on the UVSOR FEL [22]. In the first section, we review the properties of FEL oscillators and the model used [20,23], which reproduces the longitudinal behavior of SRFEL. In Section 2, the principle of the feedback system for the laser control is described by means of a theoretical model. The experimental results obtained on Super-ACO for different control parameters, are analyzed and compared to the theoretical model ones.

2 Longitudinal instabilities of storage ring free electron lasers oscillators

2.1 Underlying physical aspects

FEL are coherent tunable pulsed sources. A relativistic electron beam travelling in a periodic permanent magnetic field structure, called undulator, emits an electromagnetic wave, at the fundamental wavelength:

$$\lambda_R = \frac{\lambda_0}{2\gamma^2}\left(1+\frac{K^2}{2}\right) \quad (1)$$

[a] *Present address*: SYNCHROTRON SOLEIL, L'orme des Merisiers, B.P. 48, Saint-Aubin, 91192 Gif-sur-Yvette Cedex, France. e-mail: `christelle.bruni@synchrotron-soleil.fr`

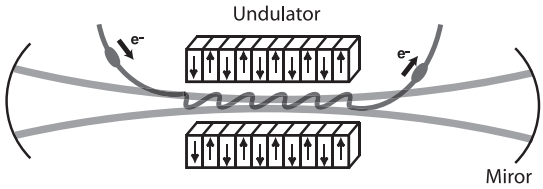

Fig. 1. The electron bunches (e^-), travelling in an undulator, emit light, which is stored in an optical cavity and is amplified, interacting with the following electron bunches.

Table 1. Characteristics of the SRFEL on Duke, ELETTRA, NIJI-IV, Super-ACO and UVSOR.

	Duke	ELETTRA	NIJI-I	Super-ACO	UVSOR
E (GeV)	1	0.9–1.3	0.26–0.31	0.6–0.8	0.5–0.6
λ (nm)	194–730	190–250	595–212	300–690	500–260
P (mW)	200	330	1	300	20–1000
G_0 (%)	∼10	10–30	5–10	1–2.5	1–2
τ_R (ns)	360	213	235	120	88.7
σ_l (ps)	2.5	2	6	10	6
σ_τ (ps)	33	12	38	89	57

with λ_0 the period of the undulator, γ the Lorentz factor of the electrons and K the deflection parameter depending on the amplitude of the magnetic field of the undulator ($K^2 \propto B_{0_z}^2$ in the case of a planar undulator, and $K^2 \propto B_{0_x}^2 + B_{0_z}^2$ in the case of a helicoidal one, z and x being the axes orthogonal to the light propagation direction). This emitted light is the spontaneous emission of the FEL. The light amplification, for a wavelength near λ_R, lies on the interaction between the relativistic electron beam and the electromagnetic wave, leading to an energy exchange. The FEL wavelength can be finely adjusted by a modification of magnetic field of the undulator. On FEL oscillators, the optical field is stored in an optical cavity, and its intensity increases non linearly until the saturation mechanism occurs when the gain is equal to the optical cavity losses ϵ (see Fig. 1).

Table 1 presents the principal characteristics of FEL, based on storage ring, and considered in this paper: the DUKE-OK4 FEL[24], the ELETTRA FEL [25], the NIJI-IV FEL [26], the Super-ACO FEL [27] and the UVSOR FEL [28]. The FEL spectral range, λ, in the UV is mainly determined by the energy E of the electrons, in the GeV range and by the characteristics of the undulator. The output power P [29] of the FEL is in the order of hundred milliwatts. The laser gain G_0 is small (in the order of the percent) and depends on the characteristic of the machine and of the insertion devices. The repetition rate of the FEL τ_R is high (in the MHz range) and is defined by the round trip time of the light pulse bouncing in the optical cavity. The rms FEL pulse duration σ_l is proportional to the square root of the rms width of the bunch longitudinal distribution σ_τ [30–32]. The UV FEL source on storage ring is presently limited to a pulse duration of the order of 2 ps and a wavelength of 190 nm.

The length of the optical resonator must be carefully adjusted to satisfy the longitudinal synchronization between the optical pulses and the electron bunches (i.e. the detuning condition). As in a storage ring the bunches are circulating identically spaced, the Free Electron Laser is pulsed at the repetition rate of the electrons in the undulator. At the millisecond time scale, the train of pulses can be continuous or can present limit cycles regimes [20]. It has been analytically demonstrated that the transition from a continuous wave, the so-called cw regime, to a pulsed regime on Storage Ring Free Electron Laser (SRFEL) occurs through a bifurcation [19]. As this transition happens close to a detuning for which the FEL has the best performances (spectral, temporal, stability, power), it is of major importance to suppress these limit cycles by stabilizing them in the steady state [15].

2.2 FEL dynamics

2.2.1 Experimental dynamics as a function of detuning

At the millisecond time scale, the temporal structure of a SRFEL can be continuous or pulsed depending strongly on the detuning δ between the round trip period of the light pulse in the optical cavity τ_R and the electrons bunch interspacing T_0:

$$\delta = \tau_R - T_0. \tag{2}$$

The perfect tuning is generally adjusted roughly with a modification of the optical length, and more finely by means of a change of the frequency of the RF cavity, which acts on the orbit length of the electrons. The RF cavity compensates the energy losses by the electrons at each turn. Figure 2 presents the macro-temporal structures of the Super-ACO FEL versus the detuning. At perfect tuning (see Fig. 2c), the laser pulse is on a steady state regime. For the detuning $\delta = 24$ fs (see Fig. 2b) and $\delta = -24$ fs (see Fig. 2d), the distribution varies on time to form macro-pulses with a frequency of a few hundred of Hertz. For larger detuning, $\delta = 84$ fs and $\delta = -52$ fs (see Figs. 2a and 2e), the laser exhibits again a steady state behavior. The time structures, between positive and negative detunings, differ in period. In fact, the frequency of the macro-pulses, which evolves in the pulsed zones [33], is smaller near perfect tuning, and then increases with the absolute value of the detuning. The pulses duration increases with the absolute value of the detuning, and is smaller for perfect tuning. The same behavior is observed on the spectral width, and the FEL can reach the Fourier limit for perfect tuning [34,35]. The evolution of the laser time structures versus detuning are summarized in Figure 3a illustrating a typical detuning curve of the Super-ACO FEL, which presents the laser intensity versus detuning. Zone 3 ($-5.6 < \delta < 2.5$ fs) corresponds to a laser around the perfect tuning condition, where the laser is cw. For small detuning, the laser presents limit cycles in the zones 2 ($-24.5 < \delta < -5.6$ fs) and 4 ($2.5 < \delta < 31$ fs). For larger detuning, the laser becomes again cw in the zones 1 ($-140 < \delta < -24.5$ fs) and 5 ($31 < \delta < 140$ fs).

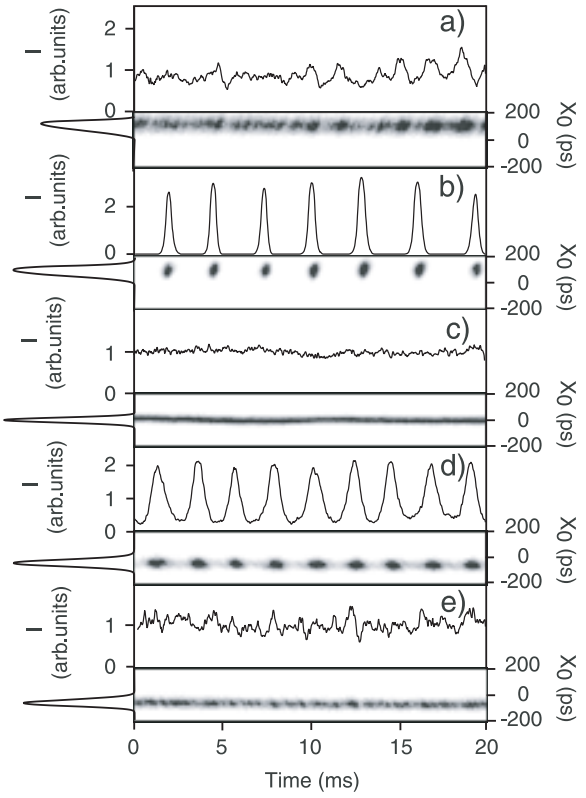

Fig. 2. Macro-pulses structures of a FEL based on a storage ring for different detuning conditions: (a) $\delta = 84$ fs, (b) $\delta = 24$ fs, (c) $\delta = 0$ fs, (d) $\delta = -24$ fs, (e) $\delta = -52$ fs. The images are taken with a double sweep streak camera (Hamamatsu $C5680$). Top of the image: horizontal cut representing the laser intensity versus time. Left of the image: vertical cut representing the laser pulse distribution. The FEL pulse width is deduced by the second order momentum of the laser pulse distribution: (a) $\sigma_l = 24$ ps, (b) $\sigma_l = 22$ ps, (c) $\sigma_l = 16$ ps, (d) $\sigma_l = 17$ ps, (e) $\sigma_l = 23$ ps. These structures have been recorded on the Super-ACO FEL with the harmonic cavity active at 90 kV: the current $I_c = 45$ mA, $G_0 = 1.8\%$, $\epsilon = 0.8\%$, energy spread in absence of laser $\sigma_0 = 10 \times 10^{-4}$, synchrotron frequency $f_s = 27.3$ kHz.

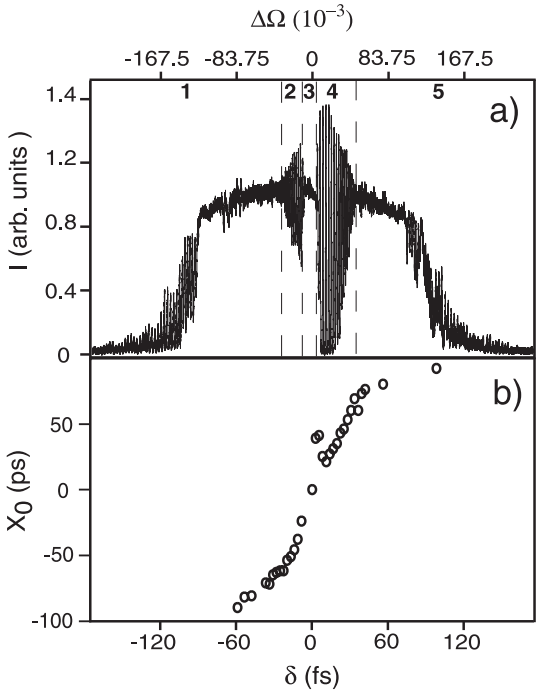

Fig. 3. (a) Detuning curve of the Super-ACO FEL: laser intensity versus detuning δ and the normalized detuning $\Delta\Omega = \delta/\epsilon\sigma_\tau$. (b) Position of the center of mass of the FEL pulse with respect to the bunch longitudinal distribution one versus detuning. In zones 1, 3, 5 the laser is cw: the laser intensity stays constant in the millisecond temporal range. In zones 2 and 4, the laser is pulsed. The experimental detuning curve is obtained by applying a slow ramp (period: 0.5 s, amplitude: 1 V) on the RF frequency pilot generator (1 V variation corresponds to a variation of 100 Hz i.e. 120 fs in terms of detuning) and detecting the laser intensity with a photomultiplier. The position of the FEL pulse center of mass is calculated by the first order momentum from a double sweep streak camera image. Experimental conditions with the harmonic cavity active at 90 kV: $I_c = 45$ mA, $G_0 = 1.8\%$, $\epsilon = 0.8\%$, $\sigma_0 = 10 \times 10^{-4}$, $f_s = 27.3$ kHz. The signals in Figure 2 corresponds respectively to the zones (a) 5, (b) 4, (c) 3, (d) 2, (e) 1.

The laser in zone 3 presents the smallest spectral and temporal width, the highest intensity stability and the largest power. These zones are generally observed on SRFEL as on the OK-4 Duke FEL [36], on Super-ACO and on UVSOR [39], whereas the zone 3 is not clearly observed on NIJI-IV [38]. In the ELETTRA [37] case, zone 3 is very tiny and it is not systematically observed because of a 50 Hz perturbation on the electron beam [25]. Table 2 illustrates the width of the different zones on the operating SRFEL. FEL near the perfect tuning exhibit a bifurcation from a steady state regime towards a pulsed regime. Here, the proposed feedback aims at increasing the laser power stability and at extending the central cw zone. As illustrated in Figures 2 and 3b, at perfect tuning the center of mass of the laser pulse corresponds to the center of mass of the longitudinal distribution of the electron bunch, and then evolves as an arctangent like function. This rapid change of the FEL position near perfect tuning has been exploited for the implementation of a so-called "longitudinal feedback", which drives back the FEL micro-pulse towards perfect tuning for compensating the FEL pulse jitter. This longitudinal feedback has been developed at Super-ACO [40] and at UVSOR [39].

2.2.2 Iterative model of the FEL

This section presents a SRFEL model based on a map that reproduces the longitudinal dynamics versus detuning of storage ring based FELs [20,23]. It constitutes our reference model for the test of the proposed feedback control.

The laser gain results from the energy exchange between the stored optical wave and a relativistic electron beam. To reinforce the coherence of the source, optical klystrons [41,42] are preferred to undulators, consisting

Table 2. Width of the different zones of the experimental detuning curve for the following FEL: Duke [36], ELETTRA [37], NIJI-IV [38], UVSOR [39], Super-ACO (see Fig. 4). ΔZ_i are the width of the zones described in Figure 3.

	Duke	ELETTRA	NIJI-IV	Super-ACO	UVSOR
ΔZ_1 (fs)	11.5	65	240	60	250
ΔZ_2 (fs)	0.5	21	120	14	19
ΔZ_3 (fs)	0.2	0	0	4.5	4
ΔZ_4 (fs)	0.5	21	120	23	19
ΔZ_5 (fs)	11.5	65	240	50	250

of two undulator sections divided by a dispersion section, where a high magnetic field is created. The gain for an optical klystron composed of planar undulators can expressed as [41,42]:

$$G_{0_{Pl}} = \frac{r_e 8\pi^{\frac{1}{4}} N_e K^2 (N\lambda_0)^2 (JJ)^2 F_f (N+N_d) f}{\sigma_x \sigma_y c \sigma_\tau \gamma^3}. \quad (3)$$

With r_e the classical radius of the electron, N_e the number of electrons, N the number of periods of one undulator section, F_f the transverse filling factor between the laser and the electron bunch [43], (N_d) the number of equivalent periods of the dispersive section, f the modulation rate of spontaneous emission depending on the energy spread σ and the residual modulation rate f_0 as $f = f_0 e^{-8\pi^2 (N+N_d)^2 \sigma^2}$ [41], σ_x and σ_y the rms width of the horizontal and vertical electron bunch distribution, c the speed of light, $(JJ) = J_0(\xi) - J_1(\xi)$ the difference of the Bessel functions of zero and first order of argument $\xi = K^2/(4+2K^2)$. For an optical klystron composed of helicoidal undulators, the gain G_{0_H} can be expressed as: $G_{0_H} = G_{0_{Pl}}/(JJ)^2$. The term JJ being lower than the unit, G_{0_H} results to be higher for the same set of parameters. As the value of gain was very low for the UVSOR FEL, the previous insertion device has been replaced by an optical klystron composed of helicoidal undulators [44], which allows a cw laser at perfect tuning to be obtained. The light amplification leads to an induced energy spread for the electron distribution, the so-called laser "heating". As a consequence the laser reaches the saturation when the gain is decreased until the cavity losses as equation (3) shows.

The Supermodes theory [30–32] explains analytically the optical pulse propagation until the saturation only for perfect tuning. A model [45] based on the evolution of the longitudinal light distribution and on the energy spread, reproduces the saturation mechanism at perfect tuning. The iterative model described in [46] reproduces the stationary output power of a SRFEL. Subsequently it has been considered that the gain depends on the detuning [20], and is equal to the losses at the border of the detuning curve. The stationary condition of the fully detuned laser intensity allows then the width of the detuning curve to be determined [47]. This numerical model neglects electron beam instabilities, and the synchrotron motion of the electrons, which oscillate around the synchronous electron (the one with the nominal energy) at the synchrotron frequency f_s and are damped according to the synchrotron damping time τ_s. Other models also take into account the transverse dynamics of the electron bunch [48,49] or the microwave instability [50,51], i.e. the interaction of the electron bunches with the vacuum chamber of the ring. To study the longitudinal dynamics of a SRFEL, let us consider in the following the numerical equations [20,23]:

$$y_n(\tau) = (1-\epsilon) y_{n-1}(\tau)[1 + G_n(\tau)] + i_s e^{\frac{-(\tau_n+\delta)^2}{2\sigma_\tau^2}} \quad (4)$$

$$\Sigma_n = \Sigma_{n-1} - \frac{2\tau_R}{\tau_s}[\Sigma_{n-1} - \int y_{n-1}(\tau) d\tau] \quad (5)$$

and

$$\Sigma_n = \frac{\sigma_n^2 - \sigma_0^2}{\sigma_e^2 - \sigma_0^2} \quad (6)$$

with

$$\tau_{n+1} = \tau_n + \delta. \quad (7)$$

This model is based on the evolution of the laser pulse intensity distribution y_n along the longitudinal coordinate τ_n centered on the center of mass of the longitudinal distribution of the electron bunch, and of the evolution of the normalized energy spread Σ_n at each pass n in the optical klystron. The normalized energy spread depends on the initial energy spread σ_0, and the one at the laser equilibrium σ_e. The laser intensity (see Eq. (4)) at the pass n, is the laser intensity at the previous pass $(n-1)$ non amplified and amplified by the term $G_n(\tau)$ taking into account the mirrors reflectivity $\sqrt{1-\epsilon}$. The last term i_s is the spontaneous emission emitted at each pass. Equation (5) describes the evolution of the normalized energy spread, which is enhanced by the laser heating and relaxes via the bunch refreshment due to the synchrotron motion. Equation (7) includes the fact that a small detuning induces a cumulative delay between the electron bunch and the laser pulse and thus reduces the longitudinal overlap. As a consequence, the laser gain is expressed as a function of the detuning δ:

$$G_n(\tau) = G_0 \frac{\sigma_0}{\sigma_n} \left[\frac{\epsilon \sigma_e}{G_0 \sigma_0}\right]^{\Sigma_n} e^{\frac{-(\tau_n+\delta)^2}{\sigma_\tau^2}}. \quad (8)$$

G_0 being $G_{0_{Pl}}$ or G_{0_H} according to the types of undulators composing the optical klystron. This model calculates in particular the time structure and the evolution of the energy spread whatever is the detuning condition.

2.2.3 Calculated detuning curve

Figure 4a shows a simulated detuning curve in the case of the Super-ACO FEL. The laser is cw in the central zone, then a bifurcation occurs, which yields to a pulsed regime, and then for large detuning, the laser becomes again cw. The model and the experiments are in qualitative agreement. Some differences can appear concerning the width

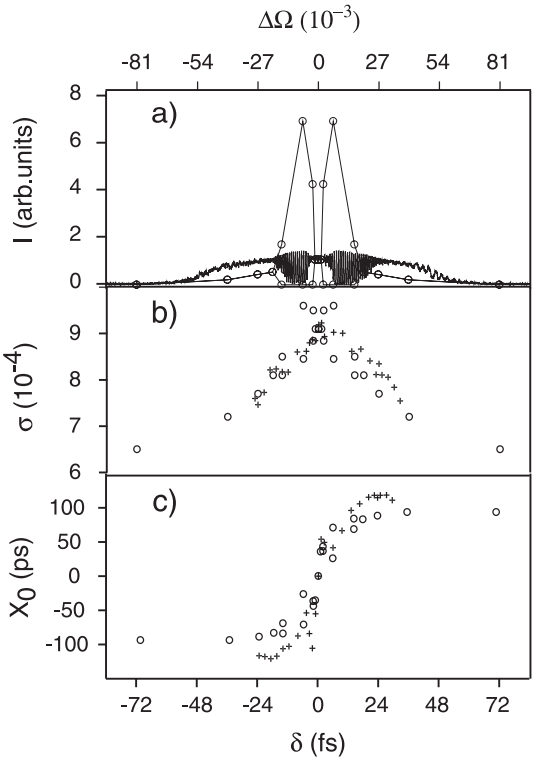

Fig. 4. (a) Detuning curve obtained in the Super-ACO case, (∘) simulated, (—) experimental. The experimental detuning curve is obtained by applying a slow ramp on the RF frequency and detecting the laser intensity by a photomultiplier. The simulated points correspond to the laser intensity in zones 1, 3 and 5, and the envelop of the minimum and maximum one in the zones 2 and 4 for each particular detuning. (b) Energy spread versus detuning, (∘) simulated, (+) experimental. The energy spread has been measured for each detuning thanks to a CCD camera, which gives the horizontal transverse electron bunch rms width σ_x linked to the energy spread σ by the following relation: $\sigma_x^2 = \varepsilon_x \beta_x + \eta_x^2 \sigma^2$ with ε_x the horizontal emittance, η_x the dispersion function and β_x the betatron function. The energy spread is a dynamical variable of the equations, and its minimum and maximum have been plotted. (c) Position of the center of mass of the laser with respect to the one of the bunch longitudinal distribution versus detuning, (∘) simulated, (+) experimental. The position is deduced from the first order momentum from a double sweep streak camera image and the simulated laser intensity distribution for each detuning. The parameters used are those listed in Table 3 for Super-ACO.

of the different zones. The width of the simulated central cw zone is smaller than in the experimental case (see Tabs. 3 and 4) probably due to a non perfect adequacy between the simulated parameters and the parameters really employed during the experiment. The experimental asymmetry of the width of the pulsed zones with respect to the detuning is explained by an asymmetry of the longitudinal distribution of the electrons, whereas the model assumes a Gaussian shape for the electron longitudinal distribution. It can be also due to the fact that the model does not include instabilities, which can affect the electron bunch as the microwave instability. Figure 4b represents

Table 3. Parameters used for the model given by equations (4) and (5). ρ is the dipole radius curvature, α the momentum compaction factor, Pl designates an optical klystron composed of two planar undulators and H of helicoidal one. The intensity of the spontaneous emission i_s is arbitrarily fixed at 10^{-9}, σ_e is deduced by the relation: $\sigma_e^2 = \sigma_0^2 - [\log(\epsilon/G_0)]/[8\pi(N+N_d)^2]$, and $\sigma_\tau = \alpha\sigma/2\pi f_s$.

	ELETTRA	Super-ACO	UVSOR
E (MeV)	1000	800	600
τ_R (ns)	216	120	88.4
ρ	5	1.7	2.2
τ_s (ms)	65	9	20
f_s (kHz)	16.1	14.3	12.6
α (10^{-3})	1.6	14.8	26
$N + N_d$	120	105	120
G_0 (%)	20	1.5	1.2
ϵ (%)	1	1	0.5
f_0	0.6	0.6	0.8
σ_0 (10^{-4})	13.5	7.5	3.4
I_c	20	40	25
OK	H	Pl	H

Table 4. Width of the different zones of the detuning curve simulated with the model given by equations (4) and (5) by using the parameters of Table 3.

	ELETTRA	Super-ACO	UVSOR
ΔZ_1 (fs)	550	54	90
ΔZ_2 (fs)	10	16	27
ΔZ_3 (fs)	0.2	2	2
ΔZ_4 (fs)	10	16	27
ΔZ_5 (fs)	550	54	90

the theoretical and experimental energy spread versus the detuning, which directly illustrates the reduction of the gain with the detuning. The lower the gain, less the laser "heats" the bunch. For the maximum gain, at perfect tuning, the enhancement of the energy spread is of 2.6×10^{-4} with respect to the value when the laser is switched off. Then, the energy spread decreases with the detuning, and reaches the "laser off" value for larger detunings. The position of the center of mass of the light pulse, with respect to the bunch longitudinal distribution one, describes an arctangent like function versus the detuning, as it is measured experimentally (see Fig. 4c). In the ELETTRA case, the model points out that it exists a central cw zone, but it is very tiny (see Tab. 4), as it is experimentally observed (see Tab. 2). The total simulated width of the detuning curve is much larger than the experimental one. Concerning the UVSOR FEL detuning curve, the central cw zone is larger in the experimental case, and the total simulated width is much lower. The model reproduces well the saturation and the longitudinal dynamics of the FEL as a function of the detuning. There is a slight disagreement due certainly to the difference between the experimental parameters, and those introduced in the model (e.g. the gain, the cavity losses or the energy spread), and the fact that the model

does not take into account the instabilities of the electrons beam [52] such as the microwave instability. As a consequence, this model can be used to point out the feasibility of an experimental suppression of the pulsed behavior under a feedback action.

This iterative model has been simplified in a system of partial differential equations, expressing the gain and the spontaneous emission in term of the cavity losses, as:

$$\begin{aligned} G_{n+1}(\tau) &= \epsilon G_n(\tau + \delta\tau_n) \\ i_s(\tau) &= \epsilon\eta G_n(\tau + \delta\tau_n) \end{aligned} \tag{9}$$

with $\delta\tau_n$ linked to the detuning $\Delta\nu_n$ by:

$$\delta\tau_n = \delta\tau_{n-1} + \tau_R^2 \Delta\nu_n. \tag{10}$$

Here the envelop of picosecond train of pulses $y_n(\tau)$, which varies slowly with the number of turn n, the cavity losses ϵ, the gain ϵG_i, and the detuning $\Delta\nu_n$ are small, thus a simplification, which is often used in the case of mode locked laser [53,54], is possible. The discreet time (macro-temporal scale) is replaced by a continuous time T expressed in unit of photon lifetime in the cavity [53]: $T = \epsilon n = \epsilon t/\tau_R$, with t the time. The dimensionless fast time (micro-temporal scale) is expressed as: $\theta = (\tau + \delta\tau_n)/\tau_R$. By realizing the following substitutions:

$$\begin{aligned} &\Delta\nu_n \rightarrow \epsilon\Delta\Omega(T)/\tau_R \\ &G_n(\tau) \rightarrow G(\theta, T) \\ &y_n(\tau) = y_n(\tau_R\theta - \delta\tau_n) \rightarrow Y(\theta, T) \\ &I_n \rightarrow I(T) \end{aligned} \tag{11}$$

and using the limited development in order of ϵ: $y_{n+1}(\tau) = Y(\theta,T) + \epsilon\partial_T Y(\theta,T) - \epsilon\Delta\Omega\partial_\theta Y(\theta,T) + O(\epsilon^2)$, one can obtain the master equations at the first order in ϵ as follows:

$$\begin{aligned} \partial_T Y - \Delta\Omega\partial_\theta Y &= -Y + G\left[Y + \eta\right] \\ \frac{d}{dT}\sigma^2 &= \kappa\left[\sigma_0^2 - \sigma^2 + (\sigma_e^2 - \sigma_0^2)I\right], \end{aligned} \tag{12}$$

with $\kappa = 2\tau_R/\epsilon\tau_s$ ($\kappa \ll 1$), and $G(\theta, T)$ defined by equation (8), where the discreet index n is replaced by the continuous time T and τ by θ, the fast time. Under these conditions, the SRFEL appears as a spatio-temporal system, where space and time are respectively defined through θ and T. The detuning effect appears as a translation given by the term $\Delta\Omega\partial_\theta y$. Figure 5 illustrates a theoretical detuning curve obtained with the differential equations using the Super-ACO parameters. In the zones 1, 3, 5, the lines represent a stable stationary regime of the laser. The laser intensity is higher in the central zone. The bifurcation occurs at the transition of the zone 3 towards zones 2 and 4, where the laser is naturally pulsed, represented by the minimum and maximum of the macro-pulses. The zones of the experimental detuning curve of Figure 3 are well reproduced.

These two iterative and continuous models reproduce the temporal structures of the laser intensity as a function of the detuning. The bifurcation between the cw and pulsed regime is clearly outlined by simulations too. This allows the action of the feedback, which should suppress the limit cycles, to be simulated.

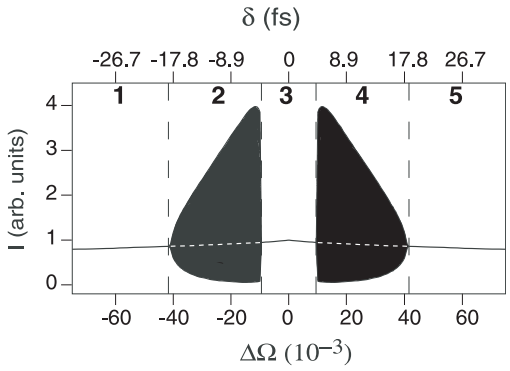

Fig. 5. Detuning curve simulated with equations (12). Zones 1, 3 and 5 correspond to a steady state regime of the laser (plain lines) whereas in the zones 2 and 4, the pulsed laser (black part corresponding to the envelop of the minimum and maximum value of the laser intensity) coexist with an unstable steady state (dash lines). Parameters are: $G_0 = 2.5\%$, $\sigma_e = 3.09\sigma_0$, $\sigma_\tau = 1$ (by choice of the unit fast time unit), $\kappa = 0.0056$, $\eta = 10^{-3}$, $\epsilon = 0.5\%$, $\tau_R = 120$ ns, $\tau_s = 8.5$ ms.

3 Stabilization

The proposed feedback is tested numerically on the iterative (see Eqs. (4) and (5)) and continuous (see Eq. (12)) equations and experimentally on the Super-ACO FEL.

3.1 Principle of the feedback system

A feedback consists in an input signal, which is modified by an electronic device to provide an output signal, which acts on a control parameter. When the laser intensity of the macro-pulse increases, the control parameter has to be perturbed by decreasing the laser gain, and contrarily when the macro-pulse intensity decreases, to force the unstable steady state to be stabilized. Previous works realized on a Nd-doped optical fiber [15] and on passively mode locked lasers [16] use the derivative of the laser intensity to perturb the laser gain and control the dynamics.

Experimentally, the FEL intensity, which can be recorded with a detector such as a photomultiplier or a photodiode, is employed as an input signal of the feedback. Several parameters can be considered to modify the FEL gain (see Eq. (3)). An orbit change of the electrons, via dipoles and quadrupoles current modifications, can be detected by fast Beam Position Monitor and modify as a consequence the filling factor. Figure 6 illustrates the electron bunch response to a sinusoidal variation of the harmonic cavity voltage of the Super-ACO storage ring. The bunch length stays almost constant (in the uncertainty of the double sweep streak camera of 4 ps during the experiment) and the center of mass of the bunch longitudinal distribution evolves sinusoidally in time. This implies that the longitudinal overlap between the laser and the electron bunches varies and changes the gain of the laser. In consequence the harmonic cavity voltage can be a control parameter for the stabilization of the pulsed zones. Finally, the detuning acts also on the longitudinal

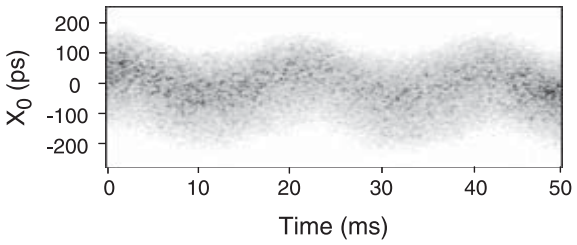

Fig. 6. Double sweep streak camera image representing the bunch longitudinal distribution in response to a sinusoidal modulation of the 500 MHz harmonic cavity voltage, (amplitude: 40 kV, frequency: 50 Hz). The camera detects the synchrotron radiation emitted by the electrons passing through a bending magnet reproducing the longitudinal distribution of the electron bunches.

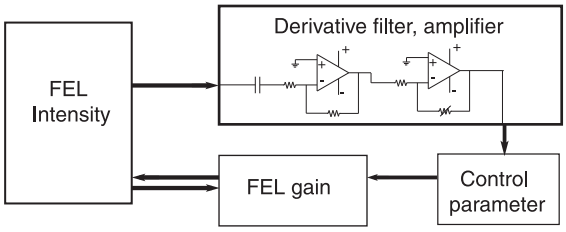

Fig. 7. Sketch of the closed loop of the feedback stabilizing the unstable steady states of the laser coexisting with the pulsed ones. The FEL intensity is detected by a photomultiplier, which rise time is too slow to resolve the picosecond pulses, but relatively rapid to detect the macro-pulses (millisecond time scale). This intensity, which is amplified and derived, varies the control parameter (RF frequency or harmonic cavity voltage), which acts on the FEL gain modifying, as a consequence, the FEL intensity.

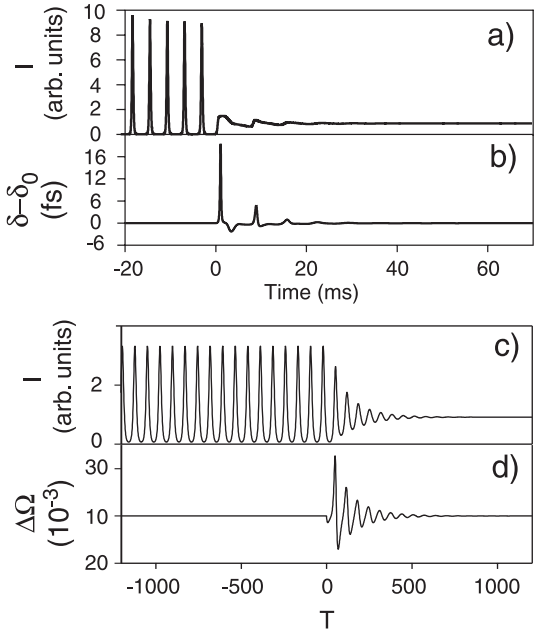

Fig. 8. Simulated feedback with the iterative model: (a) laser intensity, (b) control parameter versus time. Simulated feedback with the continuous model: (c) laser intensity, (d) control parameter versus the normalized time. The laser was first established in the pulsed zone ($\beta = 0$), and the feedback was switched on at the initial time ($\beta \neq 0$). The control parameter acts on the detuning via the RF frequency. Iterative equations conditions (see Eqs. (4) and (5)): $G_0 = 1.5\%$, $\epsilon = 1\%$, $\sigma_0 = 6.5 \times 10^{-4}$, $\delta = 2.4$ fs, $\beta = 5 \times 10^{-3}$ fs^2. Continuous equations parameters (see Eqs. (12)): $\sigma_e = 3.09\sigma_0$, $\gamma_\delta = 0.1$, $\beta = 0.1$, $\epsilon = 0.5\%$, $G_0 = 2.5\%$, $\gamma = 0.0056$, $\eta = 10^{-3}$, $\Delta\Omega_0 = 0.01$.

overlap, and can be easily changed by a variation of the frequency of the RF cavity.

The feedback system, aiming at suppressing the pulsed zones on a SRFEL, derives and amplifies the laser intensity to perturb the laser gain trough a detuning or a RF harmonic cavity voltage variation, as illustrating in Figure 7. The feedback can easily be implemented on the models (see Eqs. (4), (5) and (12)) described before.

The detuning becomes a dynamical parameter and it is expressed as a function of the derivative of the intensity as follows:

$$\delta_{n+1} = \delta_0 + \beta \frac{I_{n+1} - I_n}{\tau_R} \tag{13}$$

$$\frac{d\Delta\Omega}{dt} = \gamma_\delta \left[\Delta\Omega_0 - \Delta\Omega + \beta I_T\right], \tag{14}$$

γ_δ being the response of the electron bunch revolution frequency to a RF frequency variation, δ_0 the fixed value around which the detuning is varied, $\Delta\Omega_0$ the normalized one and β the feedback gain. Equation (13) can be implemented in the iterative model (see Eqs. (4) and (5)) and equation (14) in the continuous model (see Eqs. (12)). Figure 8 shows the effect of the control for a simulated laser previously established in its pulsed regime (negative time). When the feedback is switched on (positive time), the laser becomes cw after a transient regime during which the control parameter is damped to zero. Then, the laser is stabilized and does not need anymore the feedback system to be kept in the steady state. The different transient regime from pulsed to cw laser lies in the fact that the iterative equations do not take into account the term γ_δ and that the derivative is not exact. In the simulated detuning curve of Figure 5, the dash lines represent the stabilized solution. According to this numerical results, the stabilization of the pulsed regime can be done for a SRFEL by simply deriving the laser intensity and is possible for all the range of detuning for which the laser is pulsed.

3.2 Experimental feedback

The experimental feedback has been tested on the Super-ACO FEL with the control parameters being the RF frequency and the voltage of the harmonic RF cavity.

3.2.1 RF frequency

An analogical card has been realized to derive and amplify the laser intensity detected by a photomultiplier

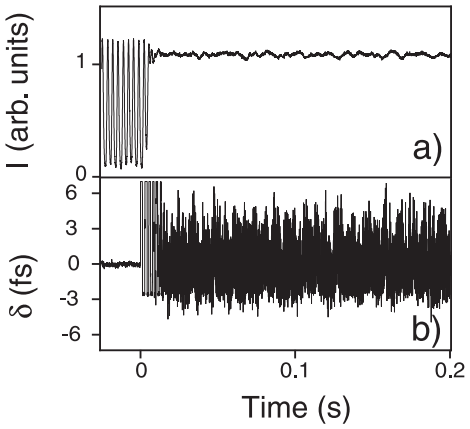

Fig. 9. Experimental feedback on the RF frequency as control parameter. (a) Laser intensity, (b) control parameter versus time. The laser was first established in the pulsed zone, and the feedback was switched on at the initial time. Super-ACO FEL experiment with the harmonic cavity active at 90 kV: $I_c =$ 46 mA, $G_0 = 1.8\%$, $f_s = 27.3$ kHz, $\epsilon = 1.2\%$, $\sigma_0 = 9 \times 10^{-4}$.

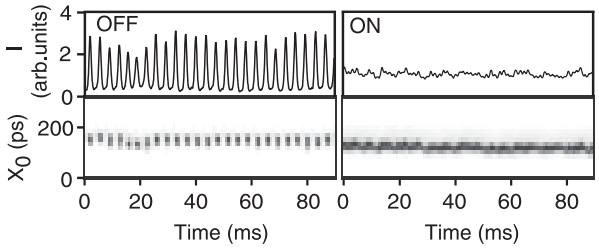

Fig. 10. Experimental feedback on the RF harmonic cavity voltage as a control parameter. Streak camera images with the horizontal cut when the feedback is switched off and on. The horizontal cut represents the laser intensity versus time. The voltage of the harmonic cavity was centered on 90 kV. The experiment was done on the Super-ACO FEL with the conditions: $I_c = 30$ mA, $G_0 = 1.7\%$, $f_s = 27.3$ kHz, $\epsilon = 1.2\%$, $\sigma_0 = 7.5 \times 10^{-4}$.

(Hamamatsu R928). For underlining the transition from pulsed to cw, the feedback can be switched on and off by putting a rectangular signal on an electronic switch. The feedback gain was found empirically during the experiment. In Figure 9, the laser is established in the pulsed zone 4 (negative time) and stabilized on a cw regime after having switched the feedback ($t = 0$). The control parameter exhibits after the stabilization some fluctuations, which maximum peak to peak amplitude is of 8 Hz in terms of RF frequency variation. After having stabilized the unstable steady states, the feedback keeps the laser cw by the corrections of the small fluctuations of intensity.

3.2.2 Harmonic cavity voltage

The stabilization has been also achieved with the RF harmonic cavity voltage as control parameter. The amplified derivative of the intensity was acting on the voltage, which was initially put at 90 kV. Figure 10, illustrating such a stabilization, represents the FEL time structures when the

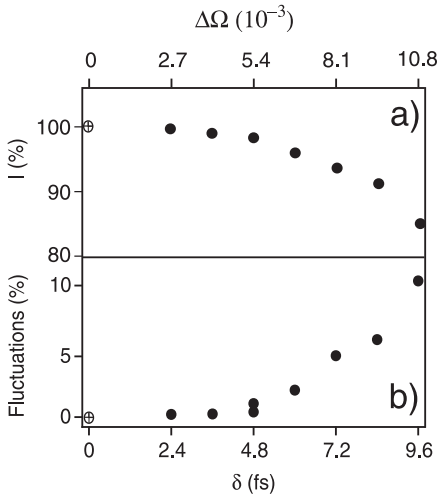

Fig. 11. (a) Laser intensity and, (b) laser intensity fluctuations versus the detuning. (⊕) cw laser obtained at perfect tuning, (•) stabilized solution of the pulsed regimes. The intensity was measured with a photomultiplier. The experiment was done on the Super-ACO FEL with the harmonic cavity active at 90 kV: $I_c = 30$ mA, $G_0 = 1.7\%$, $f_s = 27.3$ kHz, $\epsilon = 1\%$, $\sigma_0 = 7.5 \times 10^{-4}$.

feedback is alternatively switched off and on. The laser was pulsed in the zone 4, and is stabilized on the steady state when the feedback control is switched on.

A priori, the feedback can be performed with any control parameter which acts on the laser gain. A stabilization by varying the transverse orbit, which acts on the filling factor will be interesting to do. This kind of derivative feedback can be easily implanted on a storage ring FEL via any control parameter and a fast time response, to stabilize the pulsed regimes into a steady state one. As a consequence, it opens up new perspectives for FEL, which have some difficulties to maintain a cw regime at perfect tuning.

3.2.3 Detuning curve with an active feedback

Intensity and stability, which are represented in Figure 11, are one of the most important features of a laser source from an user point of view. The maximum laser intensity is obtained for the natural cw regime, in zone 3, with 100% and the stabilized steady state laser, whereas in zone 4 it has 99% (±0.3%) of amplitude for 2.4 fs of detuning, and then the laser intensity decreases as the detuning increases. For the detuning corresponding to the bifurcation, the highest laser intensity is attained for the stabilized laser. The loss of intensity of the stabilized solution compared to the natural cw regime goes from 1% to 15% depending on the detuning. The intensity fluctuations, increasing as a function of the detuning, are 0.65% for a natural cw laser and 0.89% for the stabilized solution at 2.4 fs of detuning, which corresponds to a degradation of 40% of the stability. The fluctuations attain 10.3% for the larger detuning of the pulsed zone. The stabilized solution losses intensity and some stability compared to the

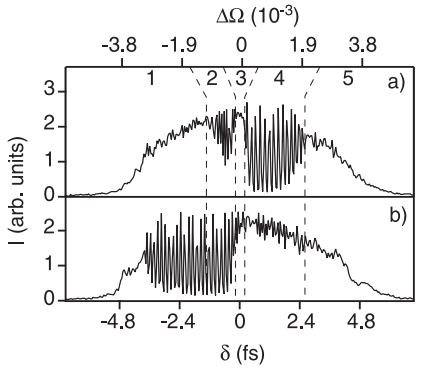

Fig. 12. Detuning curves when the feedback is switched (a) off or (b) on. To obtain such a curve with an active feedback, a slow ramp signal has been added to the derived and amplified signal of the laser intensity on the analogical card. The feedback gain was constant whatever was the detuning. The curves was done on the Super-ACO FEL with the harmonic cavity active at 90 kV: $I_c = 25$ mA, $G_0 = 1.6\%$, $f_s = 27.3$ kHz, $\epsilon = 1.4\%$, $\sigma_0 = 7 \times 10^{-4}$.

natural cw regime at perfect tuning. The stability is improved compared to the pulsed solution (100% of fluctuation) but it does not reach a so good stability as a steady state laser in zone 3. Figure 12 shows how the feedback allows the cw regime to be extended in all the detuning range. In Figure 12a, the five zones are identified again. As the zone 2 is still modulated, the control was applied on the pulsed zone 4. In this region of detuning, the feedback modifies the zone from a pulsed regime (see Fig. 12a) towards a steady state one (see Fig. 12b). Contrarily, the zone 2 becomes pulsed under the feedback action, and such a behavior is also observed for the cw zone 1. This is explained by the symmetric nature of the dynamics versus the detuning. Anyway, by changing the sign of the amplification of the derivation once the sign of the detuning is flipped, one can stabilized both pulsed zones of the detuning curve.

3.2.4 Center of mass of the FEL

Figures 13 and 14 represent respectively the experimental and simulated laser pulse distribution when the feedback is alternatively switched off and on. It allows the transition between the stabilized steady state and the limit cycle regime to be analyzed and particularly the evolution on time of the center of mass of the laser pulse. The position of the center of mass for the stabilized solution changes in comparison to the pulsed zone one. This variation is higher for a stabilized solution close to perfect tuning.

Figure 15 represents the position of the center of mass of the laser for different behaviors: natural steady state, stabilized steady state and the pulsed one. The position versus detuning exhibits an arctangent function shape for the limit cycle and the stabilized steady state solutions. In addition, the variation of position between the two coexisting solutions decreases as the detuning increases and is quasi zero for the border of the zones 4 and 5. The information on the position confirms the fact that the feedback does not perturb the gain to bring back the laser in the zone 3 of perfect tuning. Such a behavior reinforces the fact that the feedback can operate on any SRFEL.

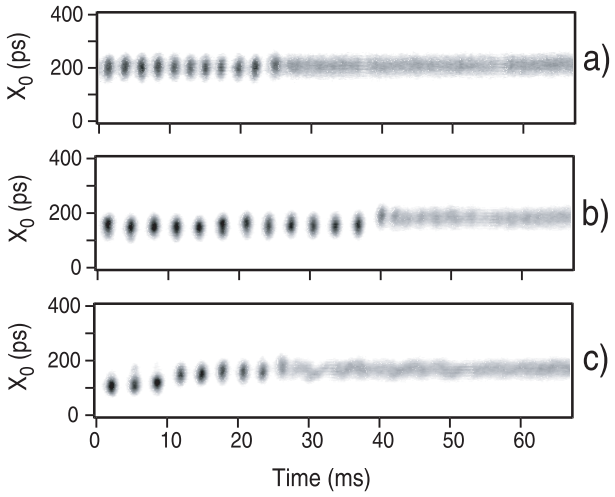

Fig. 13. Experimental double sweep streak camera image for different detuning conditions: (a) $\delta_0 \approx 12$ fs, (b) $\delta_0 \approx 4.8$ fs, (c) $\delta_0 \approx 1.2$ fs. The laser was established in the pulsed zone, and the feedback was switched on. Super-ACO FEL conditions with the harmonic cavity passive: $I_c = 40$ mA, $G_0 = 1.8\%$, $f_s = 27.3$ kHz, $\epsilon = 1.2\%$, $\sigma_0 = 9 \times 10^{-4}$.

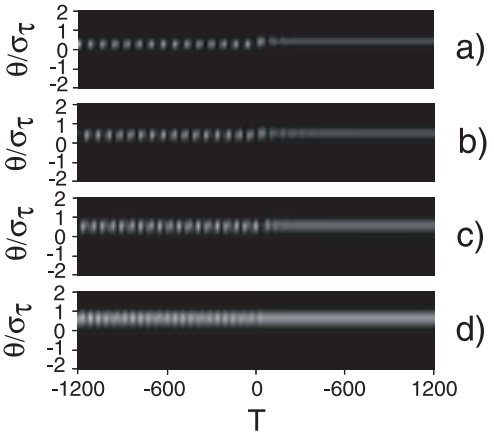

Fig. 14. Theoretical double sweep streak camera image for different detuning conditions: (a) $\Delta\Omega_0 = 0.01$, (b) $\Delta\Omega_0 = 0.02$, (c) $\Delta\Omega_0 = 0.03$, (d) $\Delta\Omega_0 = 0.04$. The laser was established in the pulsed zone, and the feedback was switched on at $T = 0$. These images have been realized with the continuous equations with the conditions: $\sigma_e = 3.09\sigma_0$, $\gamma_{\Delta\Omega} = 0.1$, $\beta = 0.1$, $\epsilon = 0.5\%$, $G_0 = 2.5\%$, $\gamma = 0.0056$, $\eta = 10^{-3}$.

4 Conclusion

We have considered the use of feedback control to extend the stability range of Storage-Ring FELs. Using the model given by equations (4) and (5) or (12), we have showed the feasibility of the suppression of the pulsed regimes by

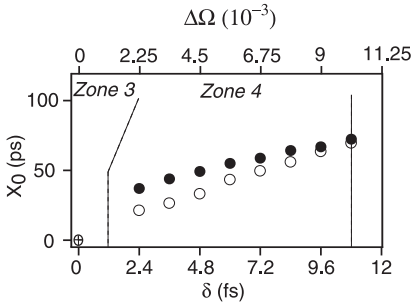

Fig. 15. Position of the center of mass of the laser pulse with respect to the bunch longitudinal distribution one versus the detuning; (•) stabilized steady state, (○) pulsed solution, (⊕) natural cw solution at perfect tuning, which position is zero. For each detuning two images have been recorded with the double sweep streak camera alternatively when the feedback was switched on and off. The position of the center of mass of the laser pulse is the first order momentum of the laser intensity distribution. Super-ACO FEL experiment with the harmonic cavity active at 120 kV: $I_c = 31$ mA, $G_0 = 2\%$, $f_s = 30.4$ kHz, $\epsilon = 1.2\%$, $\sigma_0 = 7.5 \times 10^{-4}$.

applying a feedback control, which consists in amplifying the derivative of the intensity to perturb the laser gain. The feedback system has been performed experimentally on the Super-ACO FEL for different control parameters. The stabilized steady state solution has been fully analyzed. The obtained experimental results point out the fact that the stabilized solution let the power and stability to get close to the one of perfect tuning. By analyzing the position of the center of mass of the laser pulse with respect to the bunch longitudinal distribution one, it has been demonstrated that the feedback does not bring back the laser in zone 3, but stabilizes the steady states coexisting with the pulsed one for the same parameter values. Thanks to this feedback system, the pulsed regimes are suppressed in favor of a cw laser. It extends the zone of detuning for which the laser is cw and opens up new perspective for users application on SRFEL. The feedback system should a priori be applied with the same technique on FEL, which present a pulsed regime coexisting with an unstable steady state solution. The instabilities of the electron beam may affect the stability of the FEL. As the instabilities should be different depending on the Storage Ring, the feedback system should be adjusted to the nature of the laser intensity.

The authors acknowledge J. Polian, F. Ribeiro and R. Lopes, from the RF cavity group of Super-ACO for their support on the RF cavities adjustments; the operator group of the Super-ACO storage ring and in particular B. Rieul for his help for the data acquisition; the technician, T. Guillou for his interest and help for the experiment; and R. Roux for our stimulated discussions. The CERLA is supported by the Ministère chargé de la Recherche, the Région Nord-Pas de Calais and the FEDER.

References

1. E. Ott, C. Grebogi, J.A. Yorke, Phys. Rev. Lett. **64**, 1196 (1990)
2. W.L. Ditto, S.N. Rauseo, M.L. Spano, Phys. Rev. Lett. **65**, 3211 (1990)
3. E. Hunt, Phys. Rev. Lett. **67**, 1953 (1991)
4. T.L. Carroll, I. triandaf, I. Schwartz, L. Pecora, Phys. Rev. A **46**, 6184 (1992)
5. R. Roy, T.W. Murphy, T.D. Maier, Z. Gills, E.R. Hunt, Phys. Rev. Lett. **68**, 1259 (1992)
6. S. Bielawski, D. Derozier, P. Glorieux, Phys. Rev. A **47**, R2492 (1993)
7. S. Bielawski, D. Derozier, P. Glorieux, Phys. Rev. E **49**, R971 (1994)
8. R. Meucci, W. Gadomski, M. Ciofini, F.T. Arecchi, Phys. Rev. E **49**, R2528 (1994)
9. V. Petrov, V. Gaspar, J. Masere, K. Showalter, Nature **361**, 240 (1993)
10. R.J. Wiener, D. Dolby, G.C. Gibbs, B. Smeby, T. Olsen, A.M. Smiley, Phys. Rev. Lett. **83**, 2340 (1999)
11. A. Garfinkel, M. Spano, W. Ditto, J. Weiss, Science **257**, 1230 (1992)
12. S. Boccaletti, J. Kurths, G. Osipov, D. Valladares, C. Zhou, Phys. Rep. **366**, 1 (2002)
13. Z. Gills, C. Iwata, R. Roy, Phys. Rev. Lett. **69**, 3169 (1992)
14. B. Macke, J. Zemmouri, N.E. Fettouhi, Phys. Rev. A **47**, R1609 (1993)
15. S. Bielawski, M. Bouazaoui, D. Derozier, P. Glorieux, Phys. Rev. A **47**, 3276 (1993)
16. N. Joly, S. Bielawski, Opt. Lett. **26**, 692 (2001)
17. K. Pyragas, F. Lange, T. Letz, J. Parisi, A. Kittel, Phys. Rev. E **61**, 3721 (2000)
18. S. Bielawski, C. Bruni, G.L. Orlandi, D. Garzella, M.E. Couprie, Phys. Rev. E **69**, R045502 (2004)
19. G. De Ninno, D. Fanelli, Phys. Rev. Lett. **92**, 094801 (2004)
20. M. Billardon, D. Garzella, M.E. Couprie, Phys. Rev. lett. **69**, 2368 (1992)
21. C. Bruni, M.E. Couprie, D. Garzella, G. Lambert, G.L. Orlandi, M. Danailov, G. De Ninno, B. Diviacco, M. Trovó, L. Gianessi et al., *Proceedings of the Europeen particle Accelerator conference*, p. 381 (2004)
22. S. Bielawski, C. Szwaj, C. Bruni, D. Garzella, G.L. Orlandi, M.E. Couprie, M. Hosaka, A. Mochihashi, Y. Takashima, M. Katoh et al., *Proceedings of the 27th International Free Electron laser Conference*, p. 391 (2005)
23. G. De Ninno, D. Fanelli, C. Bruni, M.E. Couprie, Eur. Phys. J. D **22**, 269 (2003)
24. P. Wang, V.N. Litvinenko, M. Emamian, J. Faircloth, J. Gustavsson, S. Hartman, S. Mikhailov, P. Morcombe, O. Oakeley, J. Patterson et al., *Proceedings of the Particle Accelerator Conference*, p. 2819 (2001)
25. G. De Ninno, M. Trovó, M. Danailov, M. Marsi, E. Karantzoulis, B. Diviacco, R.P. Walker, R. Bartolini, G. Dattoli, L. Gianessi et al., Nucl. Instrum. Meth. A **507**, 274 (2003)
26. K. Yamada, N. Sei, M. Yasumoto, H. Ogawa, T. Mikado, H. Ohgaki, Nucl. Instrum. Meth. A **483**, 162 (2002)
27. R. Roux, M.E. Couprie, R.J. Bakker, D. Garzella, D. Nutarelli, L. Nahon, M. Billardon, Phys. Rev. E **58**, 6584 (1998)

28. M. Hosaka, S. Koda, J. Yamazaki, H. Hama, Nucl. Instrum. Meth. A **445**, 208 (2000)
29. A. Renieri, Nuovo Cim. B **50**, 160 (1979)
30. G. Dattoli, T. Harmsen, A. Renieri, A. Torre, Phys. Rev. A **37**, 4326 (1988)
31. G. Dattoli, T. Harmsen, L. Mezi, A. Renieri, A. Torre, Phys. Rev. A **37**, 4334 (1988)
32. W. Colson, P. Elleaume, Appl. Phys. B **29**, 101 (1982)
33. G. De Ninno, D. Fanelli, M.E. Couprie, Nucl. Instrum. Meth. A **483**, 177 (2002)
34. M.E. Couprie, G. De Ninno, G. Moneron, D. Nutarelli, M. Hirsch, D. Garzella, E. Renault, R. Roux, C.A. Thomas, Nucl. Instrum. Meth. A **475**, 229 (2001)
35. V.N. Litvinenko, S.H. Park, I.V. Pinayev, Y. Wu, A. Lumpkin, B. Yang, Nucl. Instrum. Meth. A **475**, 234 (2001)
36. V.N. Litvinenko, S.H. Park, I.V. Pinayev, Y. Wu, Nucl. Instrum. Meth. A **475**, 240 (2001)
37. G. De Ninno, M. Trovó, M. Danailov, M. Marsi, B. Diviacco, *Proceedings of the Europeen particle Accelerator conference* p. 799 (2002)
38. K. Yamada, N. Sei, H. Ohgaki, T. Mikado, S. Sugiyama, T. Yamazaki, Nucl. Instrum. Meth. A **445**, 173 (2000)
39. S. Koda, M. Hosaka, J. Yamazaki, M. Katoh, H. Hama, Nucl. Instrum. Meth. A **475**, 211 (2001)
40. M.E. Couprie, D. Garzella, T. Hara, J.H. Codarbox, M. Billardon, Nucl. Instrum. Meth. A **358**, 374 (1995)
41. P. Elleaume, J. Phys. (Paris) **44**, C1 (1983)
42. N.A. Vinokurov, A.N. Skrinsky, Novossibirsk `Preprint INP77.59` (1977)
43. D. Nutarelli, D. Garzella, M.E. Couprie, M. Billardon, Nucl. Instrum. Meth. A **393**, 64 (1997)
44. H. Hama, Nucl. Instrum. Meth. A **375**, 57 (1996)
45. P. Elleaume, J. Phys. **45**, 997 (1984)
46. G. Dattoli, L. Giannessi, P.L. Ottaviani, A. Renieri, Nucl. Instrum. Meth. A **365**, 559 (1995)
47. G. De Ninno, C. Bruni, D. Nutarelli, D. Garzella, C. Thomas, M.E. Couprie, Phys. Rev. E **67**, 026501 (2003)
48. V.N. Litvinenko, Nucl. Instrum. Meth. A **359**, 50 (1995)
49. V.N. Litvinenko, B. Burnham, J.M.J. Madey, Y. Wu, Nucl. Instrum. Meth. A **358**, 369 (1995)
50. R. Bartolini, G. Dattoli, L. Giannessi, L. Mezi, Nucl. Instrum. Meth. A **492**, 276 (2002)
51. C.A. Thomas, J.I.M. Botman, C. Bruni, D. Garzella, M.E. Couprie, G. De Ninno, G. Dattoli, Nucl. Instrum. Meth. A **507**, 281 (2003)
52. G.L. Orlandi, C. Bruni, D. Garzella, M.E. Couprie, C. Thomas, R. Bartolini, C. Rippon, G. Dattoli, Phys. Rev. ST Accel. Beams **7**, 060701 (2004)
53. A. Dunlop, W. Firth, D. Heatley, E. Wright, Opt. Lett. **21**, 770 (1996)
54. H. Haus, J. Fujimoto, E. Ippen, J. Opt. Soc. Am. B **8**, 2068 (1991)